A protein cage system for producing bioactive peptides in *Escherichia coli*

Maxim D. Harding, [†] *Mark A. Jackson,* [†] *Edward K. Gilding,* [†] *Kuok Yap,* [†] *David J. Craik,* [†] *Frank Sainsbury,* * [‡] [¶] *and Nicole Lawrence,* * [†]

[†]Institute for Molecular Bioscience, Australian Research Council Centre of Excellence for Innovations in Peptide and Protein Science, The University of Queensland, Brisbane, Queensland 4072, Australia

[‡]Centre for Cell Factories and Biopolymers, Institute for Biomedicine and Glycomics, Griffith University, Queensland 4111, Australia

[¶]Australian Research Council Centre of Excellence in Synthetic Biology, Australia

* Correspondence: n.lawrence@imb.uq.edu.au and f.sainsbury@griffith.edu.au

KEYWORDS: bioactive peptide, virus-like particle, recombinant expression, protein encapsulation, antimicrobial resistance, bacteriophage P22.

Abstract

New therapeutics are urgently needed to curb the spread of drug-resistant diseases. Bioactive peptides (BAPs), including antimicrobial peptides, are emerging as an exciting new class of compounds with advantages over current drug modalities, especially small molecule drugs that are prone to resistance development. However, production of BAPs currently relies heavily on chemical synthesis, which is environmentally and economically costly. To address this limitation, we developed a platform that enables the biosynthetic production of BAPs via encapsulation within self-assembling protein cages in the cytoplasm of *Escherichia coli*. Using bacteriophage P22 virus-like particles (VLPs), we assessed the encapsulation of three structurally distinct classes of BAPs with activities against bacteria, cancer, and malaria. We demonstrated that encapsulation within P22 VLPs enables successful production of BAPs that are otherwise recalcitrant to recombinant expression. This approach is especially attractive for positively charged BAPs and we observed an increase in packaging efficiency within P22 VLPs that corresponded to an increase in overall positive charge. Both cyclic and linear BAPs were recovered following a simple downstream processing pipeline that involved VLP disassembly, then extraction of BAPs via enzymatic processing. This work demonstrates that encapsulation of BAPs within P22 VLPs is an effective method for biosynthetic production of BAPs in *E. coli*. By providing an alternative to chemical synthesis, this approach has the potential to increase accessibility and reduce the cost and burden of chemical waste for producing therapeutically valuable BAPs.

Introduction

The threats caused by drug resistance are increasingly evident with the spread of antibiotic-resistant bacteria, multi-drug-resistant malaria parasites, and acquired drug-resistant cancers (Tacconelli, et al., 2018, Vasan, et al., 2019, Siqueira-Neto, et al., 2023). New therapeutics, and sustainable modes of producing them, are urgently needed. Antimicrobial peptides are a promising class of therapeutics that is gaining interest for treating these drug-resistant diseases. As this class comprises a diverse range of naturally occurring molecules with activities that extend into other diseases such as cancer, they can be more broadly defined as bioactive peptides (BAPs) (Magana, et al., 2020, Muttenthaler, et al., 2021). BAPs combine the advantages of small molecule drugs, such as membrane permeability and the potential for oral bioavailability, with those of larger biologic therapies such as antibodies, which have higher metabolic stability and target specificity (Craik, et al., 2013, Wang, et al., 2022). Moreover, resistance to peptides tends to occur more slowly, if at all, compared to small molecule drugs (Peschel and Sahl, 2006, Bell, 2011, Xuan, et al., 2023, Luo, et al., 2024). This reduced likelihood of inducing drug resistance may be due to peptides acting via multiple modes of action, but is most likely explained by the larger binding interfaces between BAPs and their molecular targets, which would require accumulation of multiple genetic mutations to disrupt interactions, in contrast to small molecule drugs which can be nullified by a single genetic mutation (Podlesek and Žgur Bertok, 2020, Amiss, et al., 2022). This benefit is exemplified by BAPs that kill target cells by membrane lysis, a mechanism of action that is not only difficult to overcome by acquired resistance, but which can also bypass established drug resistance mechanisms (Rodríguez-Rojas, et al., 2014, Benfield, et al., 2024).

Production of BAPs for lab-based discovery efforts and later for scaled industrial production has predominantly been achieved using synthetic chemistry approaches like solid-phase peptide

synthesis (Wang, et al., 2022). Although chemical synthesis has enabled advances in peptide therapeutic development, excessive and harmful chemical waste from this approach has raised sustainability concerns that have triggered a movement for developing cheaper and greener production platforms (Wibowo and Zhao, 2019, Yap, et al., 2020, Roca-Pinilla, et al., 2022, Rossino, et al., 2023, Chaudhary, et al., 2024). Challenges for producing BAPs using greener recombinant expression platforms include their small size that makes them prone to proteolytic breakdown, and their biophysical properties such as high positive charge and amphipathic arrangement of charged and hydrophobic residues, which make them inherently toxic when they accumulate inside expression host cells (Li, 2011, Ishida, et al., 2016, Deo, et al., 2022). Applications of nanobiotechnology in recombinant production and metabolic engineering have recently expanded the biosynthetic range of production organisms for the manufacture of molecules of interest. For example, self-assembling protein cages have been used to compartmentalize and sequester recombinant products in *E. coli* to improve their stability and reduce toxicity (Patterson, et al., 2013, Das, et al., 2020, Su, et al., 2023), an approach we here chose to explore for BAP production.

Protein cages are nanoscale structures, comprised of one or more repeating protein subunits, that self-assemble to form a protein shell. Natural sources of protein cages include an array of independently evolved proteinaceous compartments, including viruses, ferritins, encapsulins and bacterial microcompartments (Edwardson, et al., 2022). Recombinant protein cages also comprise engineered cages, the simplest being virus-like particles (VLPs) (McNeale, et al., 2023), and a range of emerging *de novo* designed self-assembling protein compartments (Lutz, et al., 2023, Meador, et al., 2024, Yang, et al., 2024). Engineered protein cages have been used to encapsulate polypeptides such as enzymes for applications in metabolic engineering to produce valuable

heterologous small molecules (Patterson, et al., 2014, Cheah, et al., 2021, Kang, et al., 2022, McNeale, et al., 2023, Su, et al., 2023, Sator, et al., 2024), and shorter therapeutic peptides that require targeted delivery (Anand, et al., 2015, Wang, et al., 2018). In some cases, this approach has been shown to increase the yield of active proteins (Patterson, et al., 2013) or antimicrobial peptides (Lee, et al., 2020) in recombinant expression hosts. However, these examples have been demonstrated either only for a single peptide or have not successfully established downstream extraction protocols – probably due to a sub-optimal combination of encapsulating cage and respective recombinant cargo. Although covalent attachment of BAPs with protein cage coat proteins may restrict the modularity of the encapsulating system due to impacts on cage assembly (Lee, et al., 2020, McNeale, et al., 2023), a protein cage system with a large encapsulating capacity (i.e. internal cavity volume) and a non-covalent packaging mechanism would likely be best suited for developing a modular BAP encapsulating system.

Bacteriophage P22 VLPs form 58 nm icosahedral symmetries (T=7), comprising 420 coat proteins (CP) and ~100-330 scaffold proteins (SPs) (Thuman-Commike, et al., 1998). Genetic fusion of heterologous proteins to either the N- or C-terminus of the SP, or a truncated version thereof, directs cargo packaging within the VLP through non-covalent interactions with the internal face of the CP (Parker, et al., 1998, O'Neil, et al., 2011). Recently, we developed a set of expression vectors to enable rapid testing of protein cargo encapsulation within P22 VLPs in *E. coli* (Esquirol, et al., 2022). Although P22 VLPs have primarily been applied for packaging enzymes for bio-catalysis, their ability to encapsulate heterologous proteins with fast packaging kinetics that ultimately shield these molecules from the host cell, makes them an ideal system for producing potentially toxic BAPs. Previous studies have demonstrated proof-of-concept towards this goal, for example with the rescue of otherwise insoluble proteins by encapsulation within P22 VLPs,

and the recombinant packaging of BAPs such as the analgesic cone snail venom peptide MVIIA and the anticancer peptides NuBCP-9 and KLAK (Patterson, et al., 2013, Anand, et al., 2015, Wang, et al., 2018). However, in these studies the recombinant products were used in the context of the protein cage acting as a container for biocatalysis or a vehicle for therapeutic delivery, rather than as a manufacturing vessel from which the products could be successfully recovered.

Here, we successfully used P22 VLPs to produce positively charged BAPs in *E. coli*. We prototyped this system and evaluated the influence of peptide charge on BAP packaging efficiency in P22 protein cages. To demonstrate applicability of this system to a range of BAPs, we produced peptides from three structurally distinct classes: the horseshoe crab peptide tachyplesin I (TI; β-hairpin), which acts against bacteria (Edwards, et al., 2017, Amiss, et al., 2021) and its cyclic analog cTI, which acts against cancer cells (Vernen, et al., 2019, Benfield, et al., 2024); the mammalian defense peptide LL37 (α-helix), which exhibits both anticancer and antimicrobial activity (Dürr, et al., 2006, Kuroda, et al., 2015); and PDIP, a macrocyclic helix-loop-helix peptide engineered from the human defense protein platelet factor 4 with antimalarial (Lawrence, et al., 2018, Lawrence, et al., 2024) and anticancer (Lawrence, et al., 2020) activity.

Experimental Procedures

Molecular cloning

Expression plasmids were cloned as previously described (Esquirol, et al., 2022). Briefly, gene blocks for all BAPs and mRUBY3 (control fluorescent reporter) were purchased from Integrated DNA Technologies in the form of dsDNA. Primers, designed with complementary BbsI sites were also ordered from Integrated DNA Technologies for Golden Gate cloning into pBAD and pRSFDuet expression vectors, with CcdB-mediated counter selection. Clones were selected using Top 10 *E. coli* cells, with ampicillin 100 µg/mL for pBAD clones and kanamycin 50 µg/mL for pRSFDuet clones. All cloned fragments were confirmed by sequencing (Australian Genome Research Facility).

Free SP-fusion expression using pBAD

Sequenced plasmids were transformed into *E. coli* strain BL21 DE. Expression cultures were grown in LB broth supplemented with 100 µg/mL ampicillin at 37°C, with shaking at 220 rpm, until an OD_{600} of 0.6 was reached. Cultures were induced with 0.2% L-arabinose, then incubated for 16 h at 28 °C. Following overnight expression, cells were pelleted by centrifugation at 4,500 g for 15 min at 4 °C. Cell pellets were resuspended in immobilized metal affinity chromatography (IMAC) binding buffer (50 mM Tris, 300 mM NaCl pH 8, supplemented with Roche EDTA free protease inhibitors, 1 tablet per 50 mL buffer) before three passages through a cell press at 25 kpsi. Cell lysate was clarified by centrifugation at 25,000 g for 20 min at 4 °C. Free SP-fusions were then purified by IMAC using a HisTrap FF column on an ÄKTA FPLC system. Purified proteins

were desalted into phosphate buffered saline (PBS, pH 7.4) using a PD-10 miditrap column (Cytiva) and quantified using a Pierce BCA assay (ThermoFisher Scientific). Purified proteins were then analysed by denaturing sodium dodecyl-sulfate polyacrylamide gel electrophoresis (SDS-PAGE) and in-gel tryptic digest liquid chromatography tandem mass spectrometry (LC-MS/MS) on a Sciex 5600 Quadrupole Time-of-flight mass spectrometer (TOF-MS).

P22 VLP encapsulated expression using pRSFDuet

Transformed cells were grown in LB broth supplemented with 50 µg/mL kanamycin. Expression cultures were grown at 37 °C, with shaking at 220 rpm, until an OD_{600} of 0.6 was reached. Cultures were induced with 1 mM final concentration IPTG and incubated for 16 h at 28 °C. Following overnight expression, cells were pelleted by centrifugation at 4,500 g for 15 min at 4 °C. Cell pellets were resuspended in phosphate buffered saline (PBS, pH 7.4) before three passages through a cell press at 25 kpsi. Cell lysate was clarified by centrifugation at 25,000 g for 20 min at 4 °C. Clarified protein extract was then loaded onto an iodixanol density gradient (15, 20, 25%) and centrifuged at 150,000 g for 3 h at 4 °C using a Beckman Coulter L-100XP floor standing ultracentrifuge. Following centrifugation, VLPs were extracted from the bottom of ultracentrifuge tubes and desalted into PBS using a PD-10 column. VLP concentrations were calculated using a Pierce BCA assay (ThermoFisher Scientific), and then analyzed by SDS-PAGE and tryptic digest LC-MS/MS as above. To determine cargo loading, protein bands from SDS-PAGE were quantified using ImageJ (Esquirol, et al., 2022) and compared to determine the ratio of CP and SP fusion cargo. These densitometric calculations were also used in combination with the BCA assay data to calculate the recombinant yield of SP BAP fusions as mg/L of culture media.

Negative stain Transmission Emission Microscopy (TEM)

Purified VLPs were diluted to 0.25 mg/mL in PBS and applied (10 µL) to formvar/carbon coated grids (ProSciTech) for 2 min. Grids were washed three times on droplets of water for 30 seconds before staining on 10 µL of 2% uranyl acetate for 2 min. TEM was performed on a JEOL 1010 electron microscope at 80 kV operating voltage.

Extraction and processing of BAPs

VLPs purified by ultracentrifugation and desalted into PBS (approximately 3.5 mL) were diluted into 50 mL of chaotropic cargo extraction buffer (6.75 M urea, 500 mM NaCl, 50 mM Tris, 20 mM Imidazole, pH 7.4) and shaken over night at 4 °C. The disassembled VLP solution was loaded onto a HisTrap FF column (Cytiva) and SP-BAPs were purified from the P22 CP using an ÄKTA FPLC system. Samples were analyzed by SDS-PAGE following purification before buffer exchange using a PD10 column into tobacco etch virus (TEV) protease processing buffer (50 mM Tris, 1 mM DTT, 0.5 mM EDTA, pH 8.0). Buffer-exchanged SP-BAPs were then concentrated using a 3.5 kDa Amicon filter (Merck) before being quantified using a Pierce BCA assay (ThermoFisher Scientific). BAPs were then cleaved from the SP by overnight incubation with TEV enzyme variant hyperTEV60 (Sumida, et al., 2024) at 4 °C at a 1:10 (enzyme:substrate) molar ratio. Success of cleavage was assessed both by SDS-PAGE and on a Sciex 5800 matrix-assisted laser desorption/ionization (MALDI) TOF-MS. Cleaved BAPs were then purified from the reaction by reverse-phase high-performance liquid chromatography (RP-HPLC) using a Shimadzu system and a Phenomenex Jupiter C18 column with a 1% gradient from solvent A (0.005% TFA in water) to solvent B (0.05% TFA in 90% acetonitrile). HPLC fractions were assessed by electro-

spray ionization mass spectrometry (ESI-MS) and the BAP containing fractions were lyophilized. For cyclisation to produce cTI and cPDIP, the lyophilized linear peptides were resuspended in cyclisation buffer (100 mM Na_3PO_4 and 50 mM NaCl at pH 6) and incubated with modified recombinant *Oldenlandia affinis* asparaginyl endopeptidase (AEP) enzyme (*Oa*AEP1b[C247A]), as previously described (Yap, et al., 2021). Briefly, AEP enzyme and BAP substrate were incubated overnight at room temperature at a ratio of 1:10 (enzyme:substrate). Success of the overnight reaction was confirmed by MALDI TOF-MS as described above.

Results and Discussion

Protein cage construct design

With the aim of developing a reliable platform for the biosynthetic production of a range of BAPs in *E. coli*, we investigated the effect of encapsulation within P22 VLPs on BAP yield. For rapid testing of BAP expression and packaging parameters, we employed the recently developed P22 plasmid system (Esquirol, et al., 2022). This system enables Golden Gate cloning of genes into acceptor vectors such that the coding sequences are introduced in-frame with the P22 SP, fused at either the N- or C-terminus (Supplementary Table S1). The pBAD acceptor vectors contain a single open reading frame for expression of the SP fusion protein alone, whereas the pRSFDuet plasmids facilitate co-expression of the SP fusion and the P22 CP. To investigate the effect of encapsulation on recombinant yield, we compared the expression of BAPs using either the pBAD plasmid (with no P22 CP) or the pRSFDuet plasmid (with P22 CP) respectively (Figure 1).

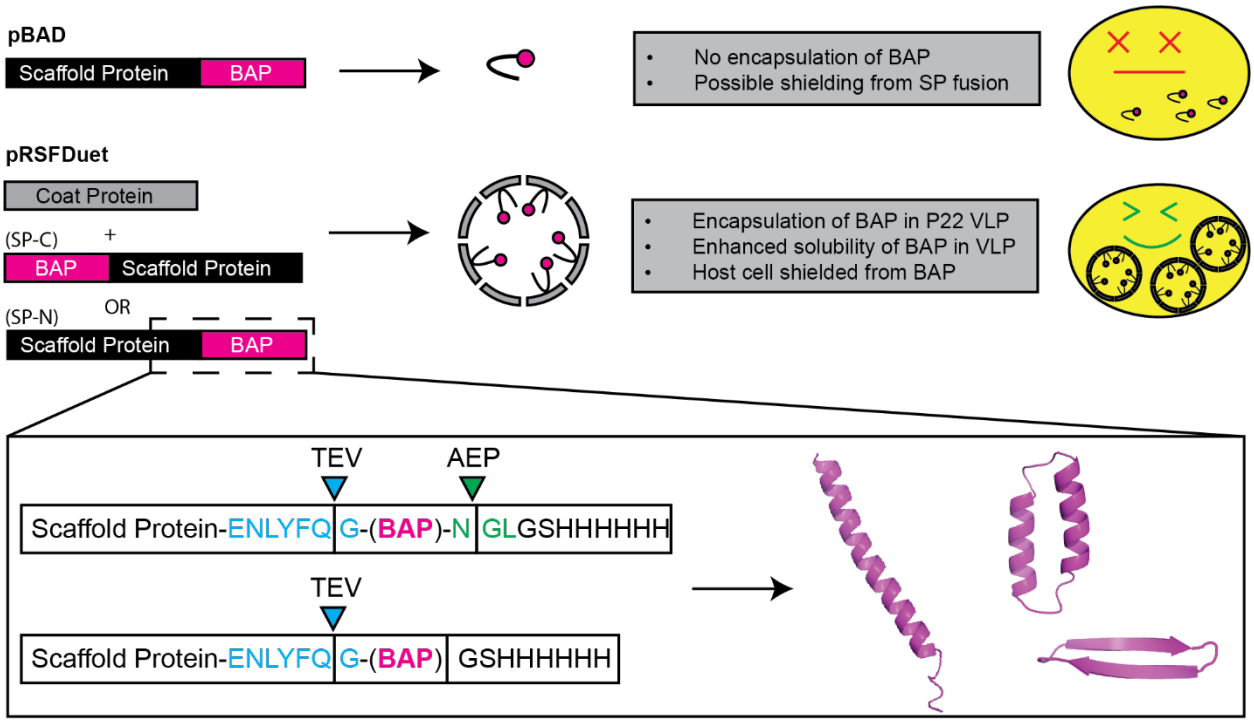

Figure 1. Protein cage construct design. pBAD vector expression results in production of a SP-bioactive peptide (BAP) fusion which will not assemble into a VLP and can result in toxicity to the *E. coli* expression host if the SP does not itself shield the host from toxic BAP characteristics. In contrast, pRSFDuet expression will co-produce both the SP-BAP fusion (either SP-N or SP-C configuration) and the P22 CP, enabling VLP assembly, BAP packaging, and shielding of *E. coli* host from toxic BAP effects. SP-BAP fusions were designed such that a range of structurally distinct BAPs could be extracted and processed from the VLP by protease cleavage *in vitro*. The tobacco etch virus (TEV) protease recognition sequence is highlighted in blue and the *Oldenlandia affinis* asparaginyl endopeptidase (AEP; *Oa*AEP1b[C247A]) recognition sequence is highlighted in green.

The protein constructs were designed to enable straightforward purification and processing steps for downstream liberation of BAPs from P22 VLPs. A hexa-histidine tag was included at either the N- or C-termini, whichever was distal to the SP among the different constructs to enable downstream chromatographic separation of the SP-BAP fusion from the P22 CP. To facilitate cleavage of BAPs from the SP-fusion, a tobacco etch virus (TEV) protease processing site was included immediately adjacent to the BAP N-terminus, enabling the cleaved BAP to retain only a single glycine (G) amino acid scar at its N-terminus. To enable peptide backbone cyclisation – a

modification employed to enhance stability and resistance to proteolytic breakdown of therapeutic peptides (Chan, et al., 2013, Craik and Du, 2017, Vernen, et al., 2019, Hayes, et al., 2021) – an asparaginyl endopeptidase (AEP) recognition sequence was included at the BAP C-terminus to enable subsequent cyclisation (Harris, et al., 2015, Yang, et al., 2017).

Evaluating the BAP protein cage system

To determine whether the P22 VLP is a suitable system for biosynthetic production of BAPs, we assembled constructs with the therapeutic antimalarial peptide candidate PDIP and the P22 SP fused to either the N-terminus or C-terminus (SP-N, SP-C; Figure 1). As a control, we produced constructs with mRUBY3 as a fluorescent reporter of expression. We first investigated the baseline expression level of SP-PDIP and SP-mRUBY3 (N-terminal SP fusions) as free protein fusions using the pBAD vector system. Expressed fusion proteins were purified using histidine-tag affinity chromatography and quantified using a BCA assay. SDS-PAGE and LC-MS/MS analysis of extracted protein bands digested with trypsin was used to confirm species identity. Recombinant yields of the expressed SP fusions were calculated by densitometric analysis using ImageJ (Esquirol, et al., 2022). SP-mRUBY3 was successfully expressed and purified, with an average yield of 2 mg/L of culture, but SP-PDIP was not detected (Figure 2A, Supplementary Figures S1 and S2). The inability to produce the SP-PDIP fusion protein was consistent with previous attempts to recombinantly produce PDIP with a range of protein fusion partners – an effect attributed to the high positive charge and preferential interaction of PDIP with negatively charged membranes (Lawrence, et al., 2018), that probably cause toxicity to the production host (Li, 2011).

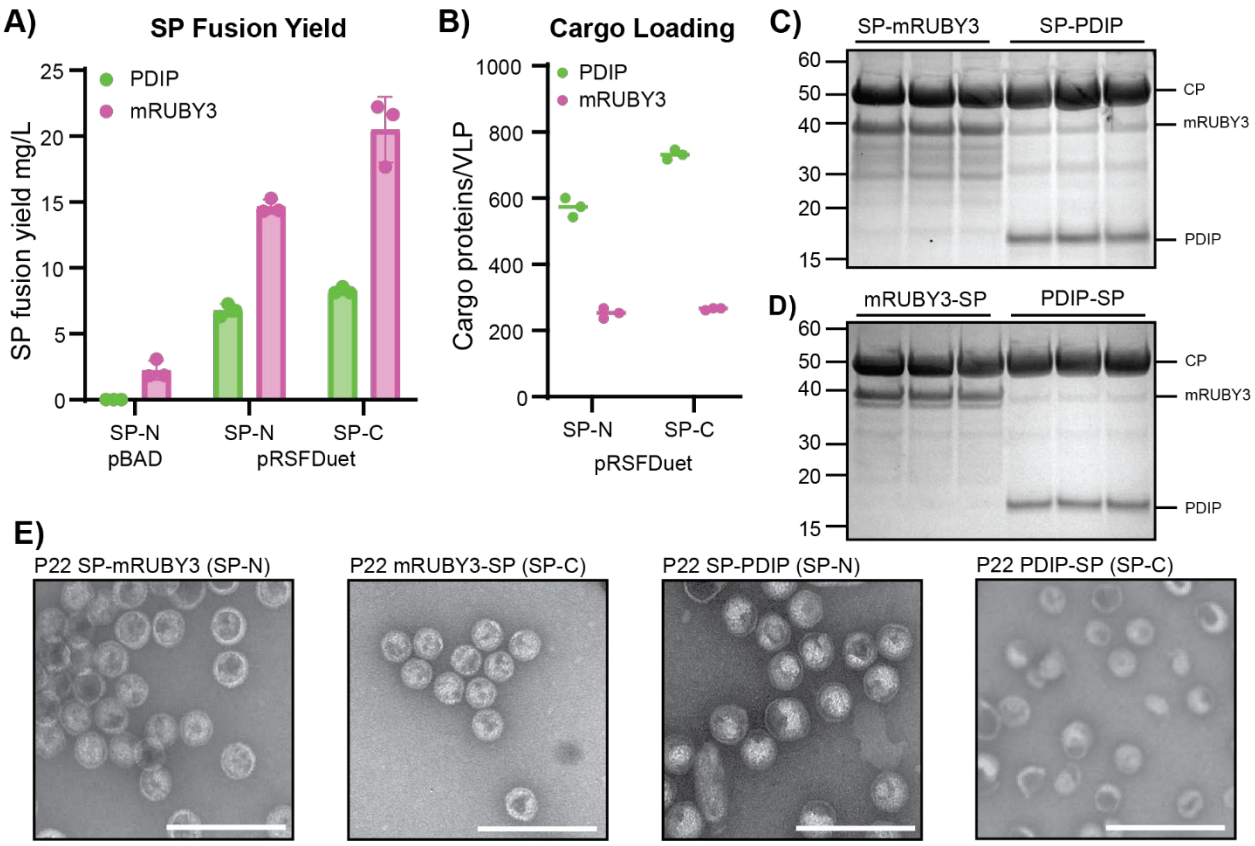

Figure 2. Prototyping P22 BAP VLPs. A) Comparison of recombinant yields of SP fusions (mg/L) expressed as free proteins using pBAD (SP-N) or as VLPs using either pRSFDuet (SP-N or SP-C). B) Calculated average loading of cargo proteins per VLP. C) SDS-PAGE for SP-N expressions for mRUBY3 and PDIP. D) SDS-PAGE for SP-C expressions for mRUBY3 and PDIP. Data in panels A-D is from three separate expressions for each construct. E) Representative negative stain TEM images for all four prototype P22 VLPs. The white scale bar is 250 nm.

In contrast to the inability to produce SP-PDIP with the pBAD expression vector, using the pRSFDuet vectors to co-express SP-mRUBY3 or SP-PDIP together with P22 CP allowed successful expression and encapsulation of both mRUBY3 and PDIP, as observed by SDS-PAGE of purified VLPs for both SP-N and SP-C fusions (Figure 2C and 2D, respectively). Correct identity of the SP-fusions and P22 CP was confirmed using tryptic digest LC-MS/MS (Supplementary Figure S2). This is the first time that the antimalarial peptide candidate PDIP has been successfully expressed in any format by *E. coli*. Moreover, packaging of SP-PDIP fusions at

572 (SP-N) and 731 (SP-C) cargo proteins per VLP was much higher than observed for SP-mRUBY3 fusions (252 and 265 cargo proteins per VLP for SP-N and SP-C respectively, see Figure 2B). The high packaging density of PDIP as both SP-N and SP-C fusions suggests favorable interactions between P22 CP and SP-fusion. This finding is consistent with the high packaging density of 543 fusion proteins per P22 VLP that was previously reported for the analgesic peptide MVIIA, which was packaged to explore delivery across the blood brain barrier (Anand, et al., 2015).

Encapsulation of the fusion proteins produced much greater yields of PDIP SP fusions (6.7 mg/L for SP-N, 8.2 mg/L for SP-C), and mRUBY3 SP fusions (14.3 mg/L for SP-N, 20.5 mg/L for SP-C) compared to those of free SP fusions (Figure 2A). Assessment of the purified particles by negative stain transmission electron microscopy (TEM) confirmed the successful assembly of P22 VLPs for each of the four prototype SP fusions (Figure 2E). Compared to purified particles packaged with mRUBY3, the VLPs with packaged PDIP displayed irregularity in particle morphology for both SP-N and SP-C orientations (Figure 2E, Supplementary Figure S3). This irregularity might be caused by the high ratio of SP-fusion to CP, which can lead to excess assembly nuclei, aberrant assembly, and formation of kinetically trapped assembly intermediates (Parent, et al., 2006). Nevertheless, the capacity to recombinantly express PDIP in this system suggests that encapsulation during expression using the P22 protein cage can effectively sequester BAP cargo to the internal lumen of the VLP. Here, encapsulation of the BAP cargo can shield the peptide from degradation by host cell proteases, and protect the host cell from toxic effects while accumulating a highly charged and membrane-active peptide such as PDIP.

Given the minor difference in recombinant yield achieved for encapsulated PDIP in either the SP-N or SP-C orientation (Figure 2A–D), further work here used the SP-N orientation only, for two

reasons. First, for linear BAPs such as LL37, removal of the SP via TEV cleavage from the SP-N orientation leaves a single glycine residue on the final product (Figure 1). Second, we found that AEP processing (cyclisation) of PDIP was inefficient when using the SP-C orientation (Supplementary Figure S4), possibly due to the intrinsically disordered nature of the SP in solution (Guo, et al., 2024), which may interfere with binding or enzyme activity (McNeale, et al., 2023).

Influence of charge on BAP packaging efficiency

The considerable difference in cargo loading between PDIP and mRUBY3 (Figure 2B) led us to investigate contributing factors. We hypothesized that the high positive charge of PDIP, rather than its reduced size compared to mRUBY3 and other previously reported proteins (O'Neil, et al., 2011), might be responsible for the high cargo loading. This would make the P22 VLP encapsulation system, with its negatively charged interior surface, particularly well-suited for packaging molecules with cationic surfaces, a common feature of many BAPs. To test this, we designed a series of charge-varied SP-PDIP constructs. By adding anionic linker sequences, comprised of 2, 4, or 6 repeating motifs of the amino acids glutamic acid and glycine (EEG), we created three SP-PDIP variants with charges of +9, +5 and +1 at pH 7.4, respectively (Figure 3A, 3B). Including the original SP-PDIP construct, this provided a series of BAP constructs with an overall charge ranging from +13 to +1. To assess the influence of overall charge on P22 VLP loading efficiency, these constructs were expressed from the pRSFDuet plasmid.

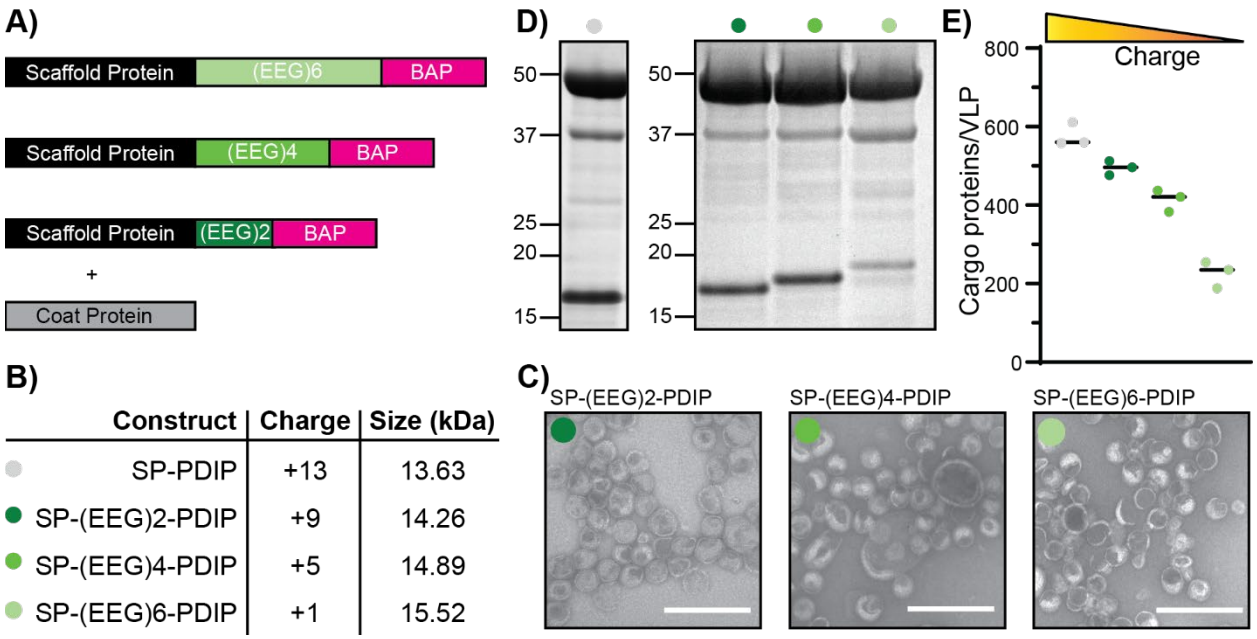

Figure 3. Effect of charge on cargo packaging. A) Constructs for anionic linker series of SP-PDIP fusions. B) The calculated charge of the constructs at pH 7.4 and size in kDa. Colour code for each construct is shown alongside construct names. C) Negative stain TEM images for SP-(EEG)2-PDIP, SP-(EEG)4-PDIP, and SP-(EEG)6-PDIP from left to right respectively. White scale bar represents 250 nm. D) SDS-PAGE image for comparison of SP-PDIP band size and intensity with anionic linker changes. E) Calculated cargo proteins per VLP from n = 3 biological replicates.

Each of the charge-varied constructs was successfully packaged into P22 protein cages as shown by negative stain TEM (Figure 3C), with their corresponding changes in mass visualised by SDS-PAGE of purified VLPs (Figure 3D) and sequences confirmed by tryptic digest LC-MS/MS (Supplementary Figure S2). Densitometric analysis of the cargo loading for each charge variant, revealed a sequential decrease in cargo loading (572, 495, 414, and 226 cargo proteins per particle on average, see Figure 3E) corresponding to a decrease in overall SP-(EEG)*n*-PDIP charge (Figure 3B). Although increasing molecular weight of the SP-(EEG)*n*-PDIP fusion proteins might contribute to the decrease in packaging density, it is more likely that reduction of the overall positive charge is responsible for this trend for several reasons. First, using the same expression vectors, we recently reported SP-fusion cargo loadings as high as 588 molecules per P22 VLP for a 55 kDa enzyme (McNeale, et al., 2023). In that case, higher than expected loading was attributed

to oligomerisation of the enzymes, but it does show that the lower loading of the charge variants was not due to the physical properties of the VLPs. Second, previous work investigating P22 SP-CP interactions and cargo retention in P22 VLPs showed that a truncated version of the P22 SP (the SP sequence used in this study) had greater affinity for the P22 CP compared to the wild-type SP (McCoy, et al., 2018). This increased affinity was also attributed to increased overall positive charge of the truncated SP compared to the wild-type. These combined observations suggest that higher positive charge of SP-BAP fusions may contribute to increased loading within P22 VLPs and that this platform is well suited for expressing and accumulating a range of cationic BAPs.

Expression of two structurally different cationic BAPs using P22 VLPs

To assess the broader applicability of the P22 protein cage system for biosynthetic production of BAPs, we tested the expression of BAPs from two additional structural classes; the linear α-helical peptide LL37 (Sancho-Vaello, et al., 2020) and a cyclic analogue of the β-hairpin peptide TI (cTI; Vernen, et al., 2019, Benfield, et al., 2024). Co-expression of both of these peptides as SP-N fusions with P22 CP (pRSFDuet system) successfully facilitated P22 VLP assembly and BAP cargo encapsulation, as shown by SDS-PAGE, negative stain TEM, and tryptic digest LC/MS-MS (Figure 4A, 4B, and Figure S2). Yields for encapsulated SP-LL37 and SP-TI were 12.3 and 3.3 mg/L of culture respectively (Figure 4C), with high density cargo loading of 634 and 990 SP fusions per particle for SP-LL37 and SP-TI respectively (Figure 4D) – further supporting the suitability of P22 VLPs for packaging cationic BAPs. Notably, neither of these BAPs was detected when expressed as free SP fusions using the pBAD vector (Figure 4C, Supplmentary Figure S1).

The cargo loading density of SP-TI (Figure 4D) was higher than observed for SP-PDIP and SP-LL37 despite these three SP-BAPs having a similar overall charge. It is possible that the more compact secondary structure (β-sheet) and slightly smaller size of the SP-TI fusions (12.2 kDa compared to 13.6 and 14.1 kDa for PDIP and LL37 respectively) might facilitate greater packaging for SP-TI than the helical SP-BAP fusions. However, this high cargo loading for SP-TI was not reflected in the yield (Figure 4C), as SP-TI had the lowest yield of all BAPs tested. TI is a potent broad spectrum antimicrobial peptide, with killing mechanisms that involve membrane permeabilizaton and also binding to DNA and RNA (Hong, et al., 2015, Edwards, et al., 2017). One possible explanation for the inverse relationship between very high cargo loading but comparatively low yield of SP-TI is that if not completely packaged, the potent antimicrobial activity of TI (Edwards, et al., 2017, Amiss, et al., 2021) may impact cell viability and reduce overal recombinant protein production. We acknowledge that the yields for SP-TI and SP-LL37 are lower than other reports for producing TI and LL37 as fusion proteins (Krahulec, et al., 2010, Panteleev and Ovchinnikova, 2017). Nevertheless, these results demonstrate an important proof-of-concept that the P22 VLP system can be used to produce structurally distinct classes of BAPs recombinantly in *E. coli*. Encapsulation within VLPs provides an expanded range of options for producing BAPs that require additional processing, as discussed further below.

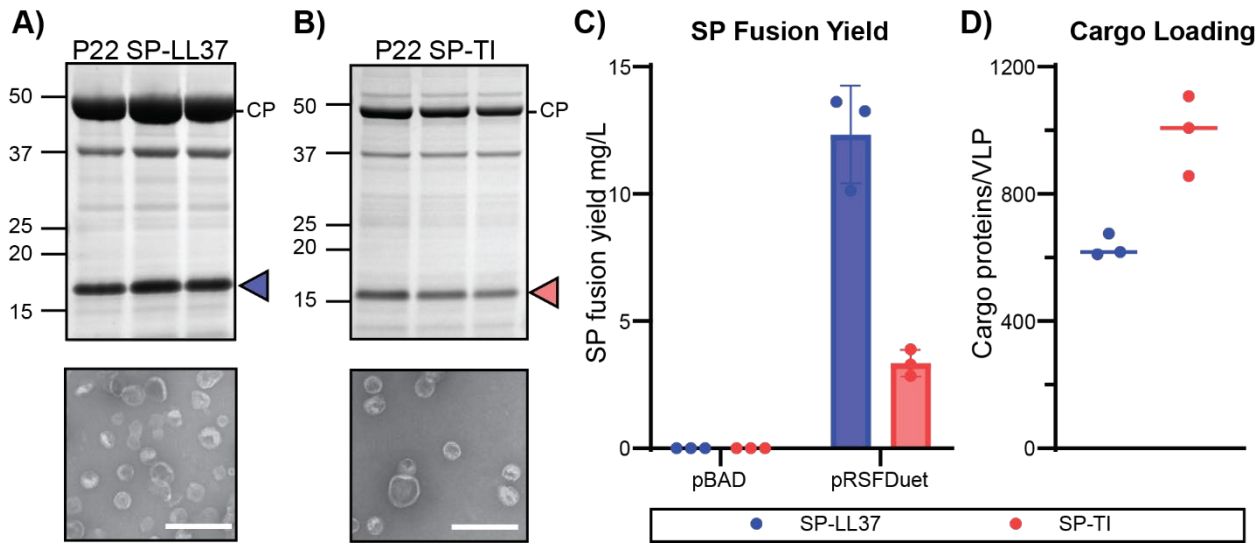

Figure 4. Encapsulation of LL37 and TI as SP fusions in P22 VLPs. A) SDS-PAGE and negative stain TEM of P22 SP-LL37. Blue arrow indicates SP-LL37. The scale bar on TEM image indicates 250 nm. B) SDS-PAGE and negative stain TEM of P22 SP-TI. Red arrow indicates SP-TI. The scale bar on TEM image indicates 250 nm. C) SP-BAP fusion yields as mg/L of culture for SP-LL37 and SP-TI expressed using either pBAD or pRSFDuet SP-N (n = 3 biological replicates). D) Calculated cargo loading for P22 SP-LL37 (blue) and SP-TI (red).

BAP processing and purification

With the aim of developing a robust and broadly accessible system for purifying BAPs from their P22 encapsulation counterparts, we designed a processing pipeline with four steps: (1) purify P22 VLPs containing SP-BAPs from total soluble protein by ultracentrifugation; (2) isolate SP-BAPs from VLPs using IMAC under chaotropic conditions that dissassemble the P22 protein cage (Capen and Teschke, 2000); (3) enzymatically cleave BAPs from SP using TEV protease; (4) purify liberated BAPs using HPLC (Figure 5A). An additional step can be included for BAPs that require further processing, for example backbone cyclization to produce cyclic peptides.

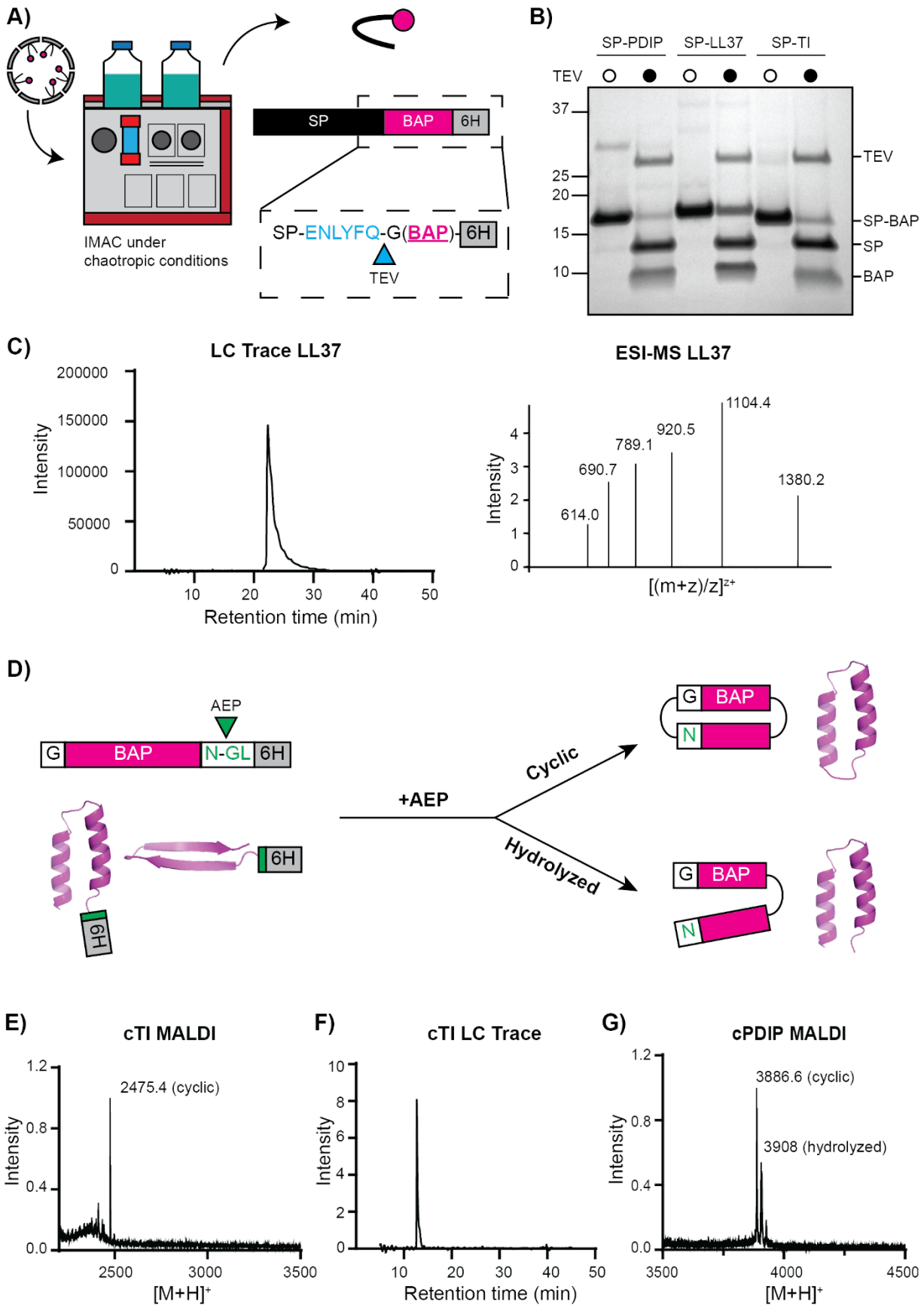
A)
IMAC under
chaotropic conditions
SP
BAP
6H
SP-ENLYFQ-G(BAP)-6H
TEV
B)
SP-PDIP
SP-LL37
SP-TI
TEV
37
25
20
15
10
TEV
SP-BAP
SP
BAP
C)
LC Trace LL37
Intensity
200000
150000
100000
50000
0
10
20
30
40
50
Retention time (min)
ESI-MS LL37
Intensity
614.0
690.7
789.1
920.5
1104.4
1380.2
[(m+z)/z]z+
D)
AEP
G
BAP
N-GL
6H
+AEP
Cyclic
Hydrolyzed
N
E)
cTI MALDI
2475.4 (cyclic)
Intensity
1.2
0.8
0.4
0.0
2500
3000
3500
[M+H]+
F)
cTI LC Trace
Intensity
10
8
6
4
2
0
10
20
30
40
50
Retention time (min)
G)
cPDIP MALDI
3886.6 (cyclic)
3908 (hydrolyzed)
Intensity
1.2
0.8
0.4
0.0
3500
4000
4500
[M+H]+

Figure 5. Post-expression processing of BAPs from P22 VLPs. A) Illustration of chromatographic separation of SP-BAP from P22 VLPs and the processing site for TEV-mediated liberation. The TEV recognition site is highlighted in blue with the N-terminal glycine residue shown. C-terminal hexa-histidine tag is also shown. B) SDS-PAGE image of TEV (hTEV60)-mediated SP-BAP cleavage for all three BAPs tested. Empty white circles above lanes indicate no added enzyme and black circles indicate addition of TEV. Respective band species are labelled along the right hand side of gel. C) LC trace of cleaved LL37 purified from the TEV cleavage reaction by HPLC and the corresponding MS signal from LC-MS. D) Illustration of AEP processing reaction. Addition of AEP to purified BAPs containing a C-terminal NGL recognition sequence can lead to one of two products: the correctly processed desired cyclic product, or a hydrolyzed linear version. E) MALDI-MS spectra of the AEP (*Oa*AEP1b[C247A]) reaction for production of cTI. F) LC trace for cTI. G) MALDI-MS spectra of the AEP (*Oa*AEP1b[C247A]) reaction for production of cPDIP.

To confirm the technical feasibility of this processing pipeline, we tested the purification and processing of all three BAPs that were expressed as SP-fusions and encapsulated within P22 VLPs in this study. Under chaotropic conditions, IMAC efficiently separated all tested SP-BAPs from P22 VLPs via binding of the C-terminal hexa-histidine tag (Supplementary Figure S5). Following buffer exchange of purified SP-BAPs into TEV processing buffer, overnight incubation with hTEV60 (Sumida, et al., 2024) successfully liberated each of the BAPs from their SP fusion partner (Figure 5B). Subjecting these TEV-cleavage reactions to HPLC successfully enabled purification of the cleaved BAPs, as characterized by LC-MS (Supplementary Figures S6, S7, and S8). This is the final processing step required for LL37, and for other linear BAPs that could be expressed using this system, as the LC trace and correct MS peaks confirmed the isolation of pure LL37 with a C-terminal hexa-histidine tag (Figure 5C). Notably, re-arrangement of the expression vector to place the histidine tag at the N-terminus of the SP would enable production of linear BAPs, with a minimal N-terminal glycine residue remaining after TEV cleavage.

Cyclization of PDIP and TI was achieved by overnight incubation of the purified linear peptides (containing C-terminal AEP recognition motif NGL) with *Oa*AEP1b[247A] enzyme at a 1:10 enzyme:substrate ratio (Yang, et al., 2017, Yap, et al., 2021) (Figure 5D). Analysis of the reaction using MADLI-TOF MS revealed complete processing of TI to produce cyclic TI (cTI) (Figure

5E), which was successfully purified using HPLC and characterized with LC-MS (Figure 5F, Supplementary Figure S9). However, MALDI-MS analysis of the PDIP reaction revealed the presence of both cyclic (cPDIP) and hydrolyzed forms (Figure 5G), that were unable to be separated using HPLC. This outcome is consistent with our attempts to cyclize other PDIP analogues that were generated via chemical synthesis. Therefore, enzyme-mediated cyclization of PDIP needs further optimization of conditions to improve the yield of cPDIP compared to hydrolyzed or unprocessed linear peptide when using AEP enzymes. Alternatively, other enzymes might provide a superior outcome for cyclizing PDIP. For example, sortase A has been used to successfully cyclize disulfide rich peptides (Jia, et al., 2014) and has even been included as a fusion partner in biosynthetic pathways to generate self-cyclizing peptides (Jia, et al., 2023).

Conclusions

In this study we produced positively charged BAPs LL37, cTI, and PDIP, by encapsulating them in bacteriophage P22 VLPs and expressing them in *E. coli*. This is the first time that PDIP, and to our knowledge cTI, have been produced biosynthetically. High packaging densities were observed for each of the SP-BAP fusions, which we demonstrated to be associated with the overall positive charge. This feature makes P22 VLPs ideally suited for packaging cationic BAPs. Correspondingly high yields were achieved for SP-PDIP and SP-LL37. However, a lower yield for SP-TI suggested incomplete shielding of *E. coli* host cells from the potent antimicrobial activity of TI. The BAPs were recovered from their expression partners (P22 SP and CP) using IMAC under chaotropic conditions, followed by cleavage from the SP fusion partner using TEV protease. LL37 with a C-terminal histidine tag was successfully purified using this approach. Incubation of linear TI with AEP ligase resulted in complete conversion to cTI, which was readily purified. However, pure

cPDIP could not be isolated from a hydrolyzed reaction by-product using this approach, suggesting the need for alternative cyclization strategies for that peptide.

By demonstrating that P22 VLPs can be successfully used to produce structurally distinct BAP classes, including linear and cyclic versions of α-helical and β-hairpin peptides, we have highlighted the potential value of this protein cage system for biosynthesis of therapeutically valuable BAPs. Accordingly, the P22 VLP encapsulation system could provide an alternative pathway to chemical synthesis, that reduces input costs and environmental burden. To improve encapsulation efficiency, and potentially the recovery yields of BAP cargo, future work could employ CP variants which endow the internal lumen of P22 VLPs with greater negative charge (Selivanovitch, et al., 2021). Additionally, given the P22 plasmid system can accommodate co-loading of different cargoes *in vivo* (McNeale, et al., 2023), co-encapsulation of SP BAP fusions and downstream processing enzymes (e.g. TEV, AEP, sortase A) could be explored to minimize *in vitro* processing requirements. Finally, with many therapeutic BAPs employing non-proteinogenic amino acids, future work could apply this P22 VLP platform in genetically expanded *E. coli* lines capable of incorporating such amino acids into BAP sequences.

Acknowledgements

This work was supported by funding from the US Department of Defense grant (PR210354 to DJC, NL, MAJ, EKG) and the Australian Research Council Centre of Excellence for Innovations in Peptide and Protein Science (CE200100012). DJC was supported by NHMRC grant (2009564). FS is supported by an Australian Research Council Future Fellowship (FT230100084) and the Australian Research Council Centre of Excellence in Synthetic Biology (CE200100029).

References

Amiss, A.S., Henriques, S.T., and Lawrence, N. (2022) Antimicrobial peptides provide wider coverage for targeting drug-resistant bacterial pathogens, *Peptide Science* **114**: e24246.

Amiss, A.S., von Pein, J.B., Webb, J.R., Condon, N.D., Harvey, P.J., Phan, M.-D., et al. (2021) Modified horseshoe crab peptides target and kill bacteria inside host cells, *Cellular and Molecular Life Sciences* **79**: 38.

Anand, P., O'Neil, A., Lin, E., Douglas, T., and Holford, M. (2015) Tailored delivery of analgesic ziconotide across a blood brain barrier model using viral nanocontainers, *Scientific Reports* **5**: 12497.

Bell, A. (2011) Antimalarial peptides: the long and the short of it, *Current Pharmaceutical Design* **17**: 2719-2731.

Benfield, A.H., Vernen, F., Young, R.S.E., Nadal-Bufí, F., Lamb, H., Hammerlindl, H., et al. (2024) Cyclic tachyplesin I kills proliferative, non-proliferative and drug-resistant melanoma cells without inducing resistance, *Pharmacological Research* **207**: 107298.

Capen, C.M., and Teschke, C.M. (2000) Folding Defects Caused by Single Amino Acid Substitutions in a Subunit Are Not Alleviated by Assembly, *Biochemistry* **39**: 1142-1151.

Chan, L.Y., Zhang, V.M., Huang, Y.H., Waters, N.C., Bansal, P.S., Craik, D.J., and Daly, N.L. (2013) Cyclization of the antimicrobial peptide gomesin with native chemical ligation: influences on stability and bioactivity, *Chembiochem: A European Journal of Chemical Biology* **14**: 617-624.

Chaudhary, S., Ali, Z., and Mahfouz, M. (2024) Molecular farming for sustainable production of clinical-grade antimicrobial peptides, *Plant Biotechnol Journal* **22**: 2282-2300.

Cheah, L.C., Stark, T., Adamson, L.S.R., Abidin, R.S., Lau, Y.H., Sainsbury, F., and Vickers, C.E. (2021) Artificial Self-assembling Nanocompartment for Organizing Metabolic Pathways in Yeast, *ACS Synthetic Biology* **10**: 3251-3263.

Craik, D.J., and Du, J. (2017) Cyclotides as drug design scaffolds*, Current Opinion in Chemical Biology* **38**: 8-16.

Craik, D.J., Fairlie, D.P., Liras, S., and Price, D. (2013) The future of peptide-based drugs, *Chemical Biology & Drug Design* **81**: 136-147.

Das, S., Zhao, L., Elofson, K., and Finn, M.G. (2020) Enzyme Stabilization by Virus-Like Particles, *Biochemistry* **59**: 2870-2881.

Deo, S., Turton, K.L., Kainth, T., Kumar, A., and Wieden, H.-J. (2022) Strategies for improving antimicrobial peptide production, *Biotechnology Advances* **59**: 107968.

Dürr, U.H., Sudheendra, U.S., and Ramamoorthy, A. (2006) LL-37, the only human member of the cathelicidin family of antimicrobial peptides, *Biochimica et Biophysica Acta* **1758**: 1408-1425.

Edwards, I.A., Elliott, A.G., Kavanagh, A.M., Blaskovich, M.A.T., and Cooper, M.A. (2017) Structure-Activity and -Toxicity Relationships of the Antimicrobial Peptide Tachyplesin-1, *ACS Infectious Diseases* **3**: 917-926.

Edwardson, T.G.W., Levasseur, M.D., Tetter, S., Steinauer, A., Hori, M., and Hilvert, D. (2022) Protein Cages: From Fundamentals to Advanced Applications, *Chemical Reviews* **122**: 9145-9197.

Esquirol, L., McNeale, D., Douglas, T., Vickers, C.E., and Sainsbury, F. (2022) Rapid Assembly and Prototyping of Biocatalytic Virus-like Particle Nanoreactors, *ACS Synthetic Biology* **11**: 2709-2718.

Guo, C., Whitehead, R.D., Struppe, J., Porat-Dahlerbruch, G., Hassan, A., Gronenborn, A.M., et al. (2024) Structural Model of Bacteriophage P22 Scaffolding Protein in a Procapsid by Magic-Angle Spinning NMR, *bioRxiv* doi: 10.1101/2024.11.01.621488.

Harris, K.S., Durek, T., Kaas, Q., Poth, A.G., Gilding, E.K., Conlan, B.F., et al. (2015) Efficient backbone cyclization of linear peptides by a recombinant asparaginyl endopeptidase, *Nature Communications* **6**: 10199.

Hayes, H.C., Luk, L.Y.P., and Tsai, Y.H. (2021) Approaches for peptide and protein cyclisation, *Organic & Biomolecular Chemistry* **19**: 3983-4001.

Hong, J., Guan, W., Jin, G., Zhao, H., Jiang, X., and Dai, J. (2015) Mechanism of tachyplesin I injury to bacterial membranes and intracellular enzymes, determined by laser confocal scanning microscopy and flow cytometry, *Microbiological Research* **170**: 69-77.

Ishida, H., Nguyen, L.T., Gopal, R., Aizawa, T., and Vogel, H.J. (2016) Overexpression of Antimicrobial, Anticancer, and Transmembrane Peptides in Escherichia coli through a Calmodulin-Peptide Fusion System, *Journal of the American Chemical Society* **138**: 11318-11326.

Jia, X., Chin, Y.K.Y., Zhang, A.H., Crawford, T., Zhu, Y., Fletcher, N.L., et al. (2023) Self-cyclisation as a general and efficient platform for peptide and protein macrocyclisation, *Communications Chemistry* **6**: 48.

Jia, X., Kwon, S., Wang, C.A., Huang, Y.H., Chan, L.Y., Tan, C.C., et al. (2014) Semienzymatic cyclization of disulfide-rich peptides using Sortase A, *Journal of Biological Chemistry* **289**: 6627-6638.

Kang, W., Ma, X., Kakarla, D., Zhang, H., Fang, Y., Chen, B., et al. (2022) Organizing Enzymes on Self-Assembled Protein Cages for Cascade Reactions, *Angewandte Chemie International Edition English* **61**: e202214001.

Krahulec, J., Hyrsová, M., Pepeliaev, S., Jílková, J., Cerný, Z., and Machálková, J. (2010) High level expression and purification of antimicrobial human cathelicidin LL-37 in Escherichia coli, *Applied Microbiology and Biotechnology* **88**: 167-175.

Kuroda, K., Okumura, K., Isogai, H., and Isogai, E. (2015) The Human Cathelicidin Antimicrobial Peptide LL-37 and Mimics are Potential Anticancer Drugs, *Frontiers in Oncology* **5**: 144.

Lawrence, N., Dennis, A.S.M., Lehane, A.M., Ehmann, A., Harvey, P.J., Benfield, A.H., et al. (2018) Defense Peptides Engineered from Human Platelet Factor 4 Kill Plasmodium by Selective Membrane Disruption, *Cell Chemical Biology* **25**: 1140-1150.e1145.

Lawrence, N., Handley, T.N.G., de Veer, S.J., Harding, M.D., Andraszek, A., Hall, L., et al. (2024) Enhancing the Intrinsic Antiplasmodial Activity and Improving the Stability and Selectivity of a Tunable Peptide Scaffold Derived from Human Platelet Factor 4, *ACS Infectious Diseases* **10**: 2899-2912.

Lawrence, N., Philippe, G.J., Harvey, P.J., Condon, N.D., Benfield, A.H., Cheneval, O., et al. (2020) Cyclic peptide scaffold with ability to stabilize and deliver a helical cell-impermeable cargo across membranes of cultured cancer cells, *RSC Chemical Biology* **1**: 405-420.

Lee, T.H., Carpenter, T.S., D'Haeseleer, P., Savage, D.F., and Yung, M.C. (2020) Encapsulin carrier proteins for enhanced expression of antimicrobial peptides, *Biotechnology and Bioengineering* **117**: 603-613.

Li, Y. (2011) Recombinant production of antimicrobial peptides in Escherichia coli: a review, *Protein Expression and Purification* **80**: 260-267.

Luo, X., Wu, Y., Zhang, X., Tang, M., Ju, F., Qin, Z., et al. (2024) Peptide-based strategies for overcoming multidrug-resistance in cancer therapy, *Chinese Chemical Letters*: 36: 109724.

Lutz, I.D., Wang, S., Norn, C., Courbet, A., Borst, A.J., Zhao, Y.T., et al. (2023) Top-down design of protein architectures with reinforcement learning, *Science* **380**: 266-273.

Magana, M., Pushpanathan, M., Santos, A.L., Leanse, L., Fernandez, M., Ioannidis, A., et al. (2020) The value of antimicrobial peptides in the age of resistance, *Lancet Infectious Diseases* **20**: e216-e230.

McCoy, K., Selivanovitch, E., Luque, D., Lee, B., Edwards, E., Castón, J.R., and Douglas, T. (2018) Cargo Retention inside P22 Virus-Like Particles, *Biomacromolecules* **19**: 3738-3746.

McNeale, D., Dashti, N., Cheah, L.C., and Sainsbury, F. (2023) Protein cargo encapsulation by virus-like particles: Strategies and applications, *Wiley Interdisciplinary Reviews: Nanomedecine and Nanobiotechnology* **15**: e1869.

McNeale, D., Esquirol, L., Okada, S., Strampel, S., Dashti, N., Rehm, B., et al. (2023) Tunable In Vivo Colocalization of Enzymes within P22 Capsid-Based Nanoreactors, *ACS Applied Materials & Interfaces* **15**: 17705-17715.

Meador, K., Castells-Graells, R., Aguirre, R., Sawaya, M.R., Arbing, M.A., Sherman, T., et al. (2024) A suite of designed protein cages using machine learning and protein fragment-based protocols, *Structure* **32**: 751-765.e711.

Muttenthaler, M., King, G.F., Adams, D.J., and Alewood, P.F. (2021) Trends in peptide drug discovery, *Nature Reviews Drug Discovery* **20**: 309-325.

O'Neil, A., Reichhardt, C., Johnson, B., Prevelige, P.E., and Douglas, T. (2011) Genetically programmed in vivo packaging of protein cargo and its controlled release from bacteriophage P22, *Angewandte Chemie International Edition English* **50**: 7425-7428.

Panteleev, P.V., and Ovchinnikova, T.V. (2017) Improved strategy for recombinant production and purification of antimicrobial peptide tachyplesin I and its analogs with high cell selectivity, *Biotechnology and Applied Biochemistry* **64**: 35-42.

Parent, K.N., Zlotnick, A., and Teschke, C.M. (2006) Quantitative Analysis of Multi-component Spherical Virus Assembly: Scaffolding Protein Contributes to the Global Stability of Phage P22 Procapsids, *Journal of Molecular Biology* **359**: 1097-1106.

Parker, M.H., Casjens, S., and Prevelige, P.E., Jr. (1998) Functional domains of bacteriophage P22 scaffolding protein, *Journal of Molecular Biology* **281**: 69-79.

Patterson, D.P., LaFrance, B., and Douglas, T. (2013) Rescuing recombinant proteins by sequestration into the P22 VLP, *Chemical Communications* **49**: 10412-10414.

Patterson, D.P., Schwarz, B., Waters, R.S., Gedeon, T., and Douglas, T. (2014) Encapsulation of an Enzyme Cascade within the Bacteriophage P22 Virus-Like Particle, *ACS Chemical Biology* **9**: 359-365.

Peschel, A., and Sahl, H.G. (2006) The co-evolution of host cationic antimicrobial peptides and microbial resistance, *Nature Reviews Microbiology* **4**: 529-536.

Podlesek, Z., and Žgur Bertok, D. (2020) The DNA damage inducible SOS response is a key player in the generation of bacterial persister cells and population wide tolerance, *Frontiers in Microbiology* **11**: 1785.

Roca-Pinilla, R., Lisowski, L., Arís, A., and Garcia-Fruitós, E. (2022) The future of recombinant host defense peptides, *Microbial Cell Factories* **21**: 267.

Rodríguez-Rojas, A., Makarova, O., and Rolff, J. (2014) Antimicrobials, stress and mutagenesis, *PLoS Pathogens* **10**: e1004445.

Rossino, G., Marchese, E., Galli, G., Verde, F., Finizio, M., Serra, M., et al. (2023) Peptides as Therapeutic Agents: Challenges and Opportunities in the Green Transition Era, *Molecules* **28**: 7165.

Sancho-Vaello, E., Gil-Carton, D., François, P., Bonetti, E.-J., Kreir, M., Pothula, K.R., et al. (2020) The structure of the antimicrobial human cathelicidin LL-37 shows oligomerization and channel formation in the presence of membrane mimics, *Scientific Reports* **10**: 17356.

Sator, C., Lico, C., Pannucci, E., Marchetti, L., Baschieri, S., Warzecha, H., and Santi, L. (2024) Plant-Produced Viral Nanoparticles as a Functionalized Catalytic Support for Metabolic Engineering, *Plants* **13**: 503.

Selivanovitch, E., LaFrance, B., and Douglas, T. (2021) Molecular exclusion limits for diffusion across a porous capsid, *Nature Communications* **12**: 2903.

Siqueira-Neto, J.L., Wicht, K.J., Chibale, K., Burrows, J.N., Fidock, D.A., and Winzeler, E.A. (2023) Antimalarial drug discovery: progress and approaches, *Nature Reviews Drug Discovery* **22**: 807-826.

Su, Y., Liu, B., Huang, Z., Teng, Z., Yang, L., Zhu, J., et al. (2023) Virus-like particles nanoreactors: from catalysis towards bio-applications, *Journal of Materials Chemistry B*.

Sumida, K.H., Núñez-Franco, R., Kalvet, I., Pellock, S.J., Wicky, B.I.M., Milles, L.F., et al. (2024) Improving Protein Expression, Stability, and Function with ProteinMPNN, *Journal of the American Chemical Society* **146**: 2054-2061.

Tacconelli, E., Carrara, E., Savoldi, A., Harbarth, S., Mendelson, M., Monnet, D.L., et al. (2018) Discovery, research, and development of new antibiotics: the WHO priority list of antibiotic-resistant bacteria and tuberculosis, *Lancet Infectious Diseases* **18**: 318-327.

Thuman-Commike, P.A., Greene, B., Malinski, J.A., King, J., and Chiu, W. (1998) Role of the Scaffolding Protein in P22 Procapsid Size Determination Suggested by T=4 and T=7 Procapsid Structures, *Biophysical Journal* **74**: 559-568.

Vasan, N., Baselga, J., and Hyman, D.M. (2019) A view on drug resistance in cancer, *Nature* **575**: 299-309.

Vernen, F., Craik, D.J., Lawrence, N., and Troeira Henriques, S. (2019) Cyclic Analogues of Horseshoe Crab Peptide Tachyplesin I with Anticancer and Cell Penetrating Properties, *ACS Chemical Biology* **14**: 2895-2908.

Vernen, F., Harvey, P.J., Dias, S.A., Veiga, A.S., Huang, Y.H., Craik, D.J., et al. (2019) Characterization of Tachyplesin Peptides and Their Cyclized Analogues to Improve Antimicrobial and Anticancer Properties, *International Journal of Molecular Sciences* **20**: 4184.

Wang, J., Fang, T., Li, M., Zhang, W., Zhang, Z.-P., Zhang, X.-E., and Li, F. (2018) Intracellular delivery of peptide drugs using viral nanoparticles of bacteriophage P22: covalent loading and cleavable release, *Journal of Materials Chemistry B* **6**: 3716-3726.

Wang, L., Wang, N., Zhang, W., Cheng, X., Yan, Z., Shao, G., et al. (2022) Therapeutic peptides: current applications and future directions, *Signal Transduction and Targeted Therapy* **7**: 48.

Wibowo, D., and Zhao, C.-X. (2019) Recent achievements and perspectives for large-scale recombinant production of antimicrobial peptides, *Applied Microbiology and Biotechnology* **103**: 659-671.

Xuan, J., Feng, W., Wang, J., Wang, R., Zhang, B., Bo, L., et al. (2023) Antimicrobial peptides for combating drug-resistant bacterial infections, *Drug Resistance Updates* **68**: 100954.

Yang, E.C., Divine, R., Miranda, M.C., Borst, A.J., Sheffler, W., Zhang, J.Z., et al. (2024) Computational design of non-porous pH-responsive antibody nanoparticles, *Nature Structural & Molecular Biology* **31**: 1404-1412.

Yang, R., Wong, Y.H., Nguyen, G.K.T., Tam, J.P., Lescar, J., and Wu, B. (2017) Engineering a Catalytically Efficient Recombinant Protein Ligase, *Journal of the American Chemical Society* **139**: 5351-5358.

Yap, K., Du, J., Looi, F.Y., Tang, S.R., de Veer, S.J., Bony, A.R., et al. (2020) An environmentally sustainable biomimetic production of cyclic disulfide-rich peptides, *Green Chemistry* **22**: 5002-5016.

Yap, K., Du, J., Rehm, F.B.H., Tang, S.R., Zhou, Y., Xie, J., et al. (2021) Yeast-based bioproduction of disulfide-rich peptides and their cyclization via asparaginyl endopeptidases, *Nature Protocols* **16**: 1740-1760.